Power System Protection and Control
ISSN:1674-3415

# REPRODUCIBILITY OF RADIOMICS FEATURES IN 68GAPSMA-11 PET/CT IMAGES OF PATIENTS WITH METASTATIC PROSTATE CANCER FOR A PERSONALIZED TREATMENT APPROACH

**Hadiseh Alimoradi[1], Kamran Aryana[2]**, Seyed Pezhman Shirmardi[3], Elham Saniei[1], Mehdi Salehi Barough[1]**

[1]Department of Medical Radiation Engineering, Central Tehran Branch, Islamic Azad University, Tehran, Iran.
[2]Nuclear Medicine Research Center, Mashhad University of Medical Sciences, Mashhad, Iran.
[3]Nuclear Science and Technology Research Institute (NSTRI), Tehran, Iran.
Hadiseh Alimoradi: hadisealimoradi99@gmail.com
Kamran Aryana: Aryanak@mums.ac.ir & Kamaryana@yahoo.com
Seyed Pezhman Shirmardi: p_shirmardi@aut.ac.ir
Elham Saniei: elhsaniei@gmail.com
Mehdi Salehi Barough: msbarough@iauctb.ac.ir & m.s.barough@gmail.com
**** Corresponding author**
Running head: "Alimoradi et al., Radiomics & PCa"

**Recevied**:22 October 2024 **Revised**: 29 November 2024 **Accepted**: 20 December 2024

***ABSTRACT*:**

**Background**: Prostate-specific membrane antigen= Positron Emission tomography (PSMA PET) images' manual interpretation can lead to a considerable number of missed metastatic Prostate cancer lesions. Therefore, Radiomics has been utilized as a novel high-potential method. However, its features lack sufficient evidence regarding their robustness and reproducibility. Consequently, we opted to assess such features in cases with metastatic Prostate cancer.

**Materials and Methods**: Our study was carried out in a tertiary referral center during 2021 and 2022 on prostate cancer cases undergoing 68 Ga-PSMA-PET/CT imaging. Initially, the PET/CT scan findings were analyzed using Python's PyRadiomics tool to extract first-order and tissue-related characteristics. Then, the segmentation of the said features was manually carried out and classified into their respective categories. Their repeatability was ultimately determined by measuring the Intraclass Correlation Coefficients (ICCs).

**Results**: A total of 150 PSMA-PET/CT images were investigated, leading to the extraction of 101 features, among which 1, 3, and 10 had excellent, good, and moderate repeatability, respectively. Out of all the ICC values, only three were statistically significant. These values were for Low Gray-Level Run Emphasis (LGLRE; ICC = 0.799, p = 0.047) and Long-Run Low Gray-Level Emphasis (LRLGLE; ICC = 0.801, p = 0.045) in the Gray-level run length matrix as well as Low Gray-Level Emphasis (LGLE; ICC = 0.906, p = 0.003) in the Gray-level dependence matrix.

**Conclusion**: Several PSMA-PET/CT-derived radiomics features have significant metastasis-predicting values in metastatic Prostate cancer. However, future studies must assess the agreement between these features and clinical and histological parameters.

***Keywords**: Prostate cancer; Ga-PSMA-PET/CT Radiomics; reproducibility; intraclass correlation coefficient (ICC).*

## INTRODUCTION

As one of the most common malignant tumors in male cancer statistics, Prostate cancer (PCa) should be suspected if the results of a digital rectal examination are indicative or if there is an increase in prostate-specific antigen (PSA) levels in the blood after which it is recommended to perform a transrectal ultrasonography (TRUS) guided biopsy to confirm the presence of any abnormal tissue [1]. In addition, although therapy has shown significant success rates, the death rates of the disease remain elevated, while also 20-50% experience recurrence during follow-up. [2].


**DOI:** 10.46121/pspc.52.4.6

Power System Protection and Control
ISSN:1674-3415

Nevertheless, the invasive nature of prostate biopsies is linked to adverse events, including pain, hematuria, and infection. Therefore, imaging techniques like magnetic resonance imaging (MRI) and computed tomography (CT) have been introduced. These modalities offer valuable information regarding the localization and staging of PCa [3]. Nevertheless, the accuracy of this information is demonstrated to be adequate when considering the molecular data obtained from Positron Emission Tomography (PET) [4].

In addition, Positron Emission Tomography (PET), utilizing 68 Ga-PSMA as the radiotracer, along with Computed Tomography (CT) (PET/CT), has become a valuable and accurate method for screening and diagnosing metastases in PCa [5]. Thus, Ga68-PSMA-PET/CT imaging has been widely accepted as the most reliable method for reevaluating recurrent PCa. Moreover, increasing evidence suggests that it can effectively replace routine imaging for the initial staging of high-risk patients [6]. However, the interpretation of images in Ga68-(PSMA) PET-CT imaging is usually carried out manually and via visual assessment by specialists and based on their experience, potentially leading to misdiagnosing many intraprostatic and metastatic lesions due to their small size or shape [7].

Radiomics is a newly developed approach that extracts quantitative data via computational methods on various imaging modalities, including PET, MRI, CT, and molecular hybrid imaging. These numerical measurements are then used to create prediction models, which help diagnose, plan treatment, and predict outcomes of various cancer and neurological disorders [8]. Nevertheless, despite its numerous advantages, most radiomics features suffer from a lack of uniformity and heterogeneity in segmentation, pre-processing settings of images, and machine learning pipeline. This limitation hinders their reproducibility, particularly in the case of PCa [4].

Moreover, the most common limitation of previous studies on radiomics in metastatic PCa was their lack of validation on external datasets [1]. Hence, our objective was to assess the resilience and consistency of radiomics characteristics in response to variations in the size, number, location, and shape of the lesions depicted in Ga68-PSMA-PET/CT images.

## MATERIALS AND METHODS

### Study Design

The following retrospective analysis was conducted on the records of patients with prostate cancer (PCa) available at our PET/CT center during the two years leading up to the initial phase of the study. We obtained the necessary permits from relevant institutional bodies, including technical and ethical protocol approval from the Institutional Review Board (IRB).

Our study was carried out in three phases. We retrospectively selected eligible patients for analysis in phase one and obtained their PET-CT images. In phase two, we performed radiomics analysis, which consisted of five steps: image pre-processing, image acquisition, feature extraction, feature classification, and descriptive feature analysis. In phase three, we investigated the reproducibility of the extracted features. (Figure 1)
[Figure 1]

### Population

The study included patients with metastatic prostate cancer who had a positive result for metastasis on Ga68-PSMA PET/CT imaging during the specified period. Patients with a confirmed diagnosis based on biopsy, elevated serum PSA, and a history of receiving targeted therapy before the PET/CT scan (such as surgical removal, chemotherapy, or radiotherapy) were included. However, patients with primary non-metastatic benign or malignant lesions in their liver, kidneys, spine, and other possible metastatic sites of prostate cancer were excluded. The study documented the age, weight, PSA level at diagnosis and its latest levels, prostate cancer staging phase (initial staging or restaging), and the anatomic locations of all segmented volumes for the included individuals.

### Sample size determination

The sample size was determined using the intraclass correlation coefficient (ICC) as a basis, as described by Bonett [9], the formula for which is brought below (where $z = 1.92$, $k = 2$, $\omega = 0.09$ and $\rho = 0.85$).

$$n = 8z_{\alpha/2}^2\{(1-\tilde{\rho}_1)^2(1+(k-1)\tilde{\rho}_1)^2\}/\{k(k-1)w^2\}+1$$


DOI: 10.46121/pspc.52.4.6

Moreover, the values required for the formula were obtained from similar studies [10, 11]. Therefore, with the significance level for ICC assumed at 0.85 and the study's statistical power of 0.95, along with a type 1 error of 0.05, a minimum sample size of 120 cases was determined. In addition, by considering a 20% dropout rate in the sample, a final sample size of 150 cases was calculated.

**Imaging protocols and settings**

The imaging process was conducted using a specific 64-slice PET/helical CT scanner, the Philips Ingenuity PET/CT Time–of–Flight system (United States). The CT scanner was set to the following parameters: tube voltage of 140 kVp, tube current of 800 mAmax, matrix size of 512 × 512, and voxel size of 1.37 × 1.37 × 3.75 mm3. Moreover, the PET scanner (matrix = 256 × 256) had a collection time of 90 seconds per bed, with 10 beds required for a whole-body scan. In addition, the 68Ga-PSMA PET radiotracer (2-2.2 MBq/kg) was injected intravenously in a single dose 60 minutes before the scans.

**Image Segmentation**

Once PET/CT scans were uploaded to mat Radiomics 1.5, image segmentation was manually performed to extract PCa volumes. For this purpose, an experienced Nuclear Medicine specialist manually performed the diagnostics using slice-by-slice delineation. The Digital Imaging and Communications in Medicine (DICOM) data, which consist of a complete set of CT images, and the 68 Ga-PSMA PET/CT pictures were loaded and segmented using the standard segment editor tool, 3D slicer (Figure 2) [12].
[Figure 2]

Furthermore, the metastatic target sites/organs, including the liver, lumbar vertebrae, pelvis, and distant lymph nodes such as femoral, left iliac, parailiac, and abdominal lymph nodes, were manually identified and segmented in each patient using PET/CT imaging.

**Feature Extraction**

We repeatedly extracted each image's features using manual segmentations, then computed them using PyRadiomics version 2.02 and integrated them into the matRadiomics software [13]. In addition, features were extracted using Laplacian of Gaussian (LOG) sigma values ranging from 0.5 to 5 with 0.5 increments, Wavelet decomposition (WAV), and a Bin width of 20. Other parameters were left to default.

Afterward, a total of 101 characteristics were derived from the dataset. The features were further classified into three categories consisting of (1) Shape and morphology-based, (2) First Order Statistics, and (3) Texture. Additionally, the latter features were classified into distinct categories, consisting of the gray level dependence matrix (GLDM), neighboring gray-tone difference matrix (NGTDM), gray level run length matrix (GLRLM), gray level size zone matrix (GLSZM), and gray level co-occurrence matrix (GLCM). (Table 1)

[Table 1]

**Feature Robustness**

Following the extraction of features, each feature had its Intraclass Correlation Coefficient (ICC) computed to measure the degree of consistency between observers and assess the reliability of the features while utilizing three different segmentation approaches.

Furthermore, the ICC value was calculated using McGraw and Wong's formula to assess absolute agreement, where ICC = MSR − MSE. The formula (2) calculates the value of MSR by adding the product of (k - 1) and MSE, the product of k, n, and the difference between MSC and MSE. In this formula, MSR represents the mean square for rows, MSE represents the mean square error, MSC represents the mean square for columns, k represents the number of observers engaged, and n represents the number of subjects. The variable j denotes the j-th feature, and KClass represents each class's total number of features [14]. Consequently, the average of ICCs was determined after grouping features according to their category using the formula below. This act resulted in generating mean ICC values for radiomics features in the Shape, FOS, GLCM, GLDM, GLRLM, GLSZM, and NGTDM categories:

ICCClass = 1 KClass ∑ KClass j=1 ICCj
Furthermore, the ICC value spans from 0 (indicating absence of reproducibility) to 1 (indicating flawless reproducibility). Furthermore, adhering to the standards set forth by Koo and Li [15], ICC values < 0.5, between


**DOI:** 10.46121/pspc.52.4.6

0.5 and 0.75, between 0.75 and 0.9, and > 0.9 indicated poor, moderate, good, and excellent feature reproducibility, respectively.

**Statistical Analysis**

Using the 26th version of the SPSS statistical software (IBM Corp. Released 2019. IBM SPSS Statistics for Windows, Version 26.0. Armonk, NY: IBM Corp). Given that the data did not follow a normal distribution (determined by the Kolmogorov-Smirnov test), we employed the Kruskal-Wallis test to determine whether the feature classes (Shape and morphology, FOS, GLCM, GLRLM, GLSZM, GLDM, and NGTDM) had a statistically significant effect on the ICC values for each image type (original, LoG, wavelet). Furthermore, 95% confidence intervals were computed for each model's performance by 1000 bootstraps. $p < 0.05$ were considered statistically significant.

## RESULTS

**Clinical Data**

We obtained PET-CT images from 150 patients averaging 68.6 ± 7.08 years suffering from metastatic PCa in various stages. Moreover, they weighed 73.19 ± 10.46 kg and had a mean PSA level of 6.5 ± 12.2 ng/ml at PCa diagnosis. In addition, the majority were in the restaging stage (79.3%) and had a positive history of prostatectomy (60%), while most had a latest PSA level below 20 ng/ml. Other relevant characteristics of these individuals are brought in Table 2.
[Table 2]

**Feature Robustness**

Among the 101 radiomic features extracted and deemed robust, 18 features belonged to the FOS category, 23 to the GLCM, 16 to the GLRLM, 14 to the shape and morphology, 15 to the GLSZM, 12 to the GLDM and 5 to the NGTDM.

***Feature Reproducibility***

Evaluating the reproducibility of the extracted features revealed that three had significant reproducibility. These features included Low Gray-Level Run Emphasis (LGLRE) (ICC = 0.799, p = 0.047) and Long-Run Low Gray-Level Emphasis (LRLGLE) (ICC = 0.801, p = 0.045) from the GLRLM category, along with Low Gray-Level Emphasis (LGLE) (ICC = 0.906, p = 0.003) from the GLDM category. (Table 3)
[Table 3]

Low Gray Level Emphasis (ICC = 0.906) had excellent reproducibility when assessed based on their reproducibility grade. Moreover, Long Run Low Gray Level Emphasis (ICC = 0.801), Low Gray Level Run Emphasis (ICC = 0.799), and Short Run Low Gray Level Emphasis (ICC = 0.79) had good reproducibility. Furthermore, 10 features, consisting of Large Dependence Low Gray Level Emphasis (ICC = 0.747), Uniformity (ICC = 0.682), Minor Axis Length (ICC = 0.628), Mesh Volume (ICC = 0.589), Run Length Non-Uniformity (ICC = 0.588), Voxel Volume (ICC = 0.588), Maximum Probability (ICC = 0.561), Minimum (ICC = 0.552), Surface Area (ICC = 0.533), and Run Percentage (ICC = 0.521) had moderate reproducibility. However, the rest had poor reproducibility. (Figure 3)
[Figure 3]

## DISCUSSION

As the 68 Ga-(PSMA) PET-CT image analysis is carried out manually and primarily based on experience, many PCa primary and secondary lesions could remain undetected [7]. However, radiomics models, as a novel method of quantifying computerized values derived from imaging, have not yet found significant application in the clinic, with their robustness and reproducibility needing to be determined first [16]. Hence, this study aimed to determine the most reliable characteristics of metastatic PCa. The findings revealed that among the 101 features analyzed, 14 exhibited a moderate to high level of reproducibility. Notably, the features of Low Gray-Level Emphasis, Long-Run Low Gray-Level Emphasis, and Low Gray-Level Run Emphasis demonstrated statistically significant ICC values.

In our study, Low Gray-Level Run Emphasis and Long-Run Low Gray-Level Emphasis of the GLRLM category had moderate reproducibility. In addition, low gray-level emphasis from the GLDM category had excellent and


**DOI:** 10.46121/pspc.52.4.6

significant reproducibility. However, this feature was the only one with excellent reproducibility. A study assessed the strength of features extracted by manual and semi-automatic segmentation of a 3D MRI prostate model, finding that gray-level texture-based features exhibited high interclass correlation coefficients (ICCs) and showed good to excellent reproducibility [17]. Similarly, another study showed that gray-level texture-based features performed better than FOS and Shape and morphology-based features, stating that shape and morphology-based were the most sensitive to the segmentation method [10]. Nevertheless, this issue highlights the importance of further investigating features based on semi-automatic and automatic segmentation.

In addition, although several other features from FOS, GLCM, Shape and morphological features, GLSZM, and NGTDM categories had moderate or good reproducibility, their analyses were not statistically significant. However, it has been reported in a systematic review that FOS features provide the most robust results among the radiomics features, even though the Uniformity feature was the only one with good reproducibility [18]. Moreover, Kurtosis, another feature of FOS, showed significant reproducibility according to another study and had a high prognostic value in predicting the survival of patients with PCa [19]. In another study, the GLSZM feature High Gray-level Emphasis was also determined to have high reproducibility, accurately distinguish tumors with a Gleason score higher than eight, and predict the involvement of distant lymph nodes [20]. Among the GLCM category, Entropy-based features also demonstrated high reproducibility for PSA changes, PCa diagnosis, and recurrence [21]. Additionally, another study found that Histo_Entropy, a measure of entropy-based tissue properties, demonstrated the highest sensitivity and specificity in identifying metastatic PCa. However, Small-zone Low Grey-level Emphasis and HISTO_energy Uniformity showed the most substantial predictive values for lymph node involvement [22].

Furthermore, analyzing radiomic characteristics in PSMA-PET/CT images across multiple studies has produced diverse outcomes due to variations in device types, settings, image acquisition techniques, segmentation methodologies, and definitions of tissue features. Consequently, interpreting the results poses a challenge [18, 23-25]. Furthermore, in contrast with previous studies, we focused more on PCa metastasis to lymph nodes and potential target organs, which can explain the differences in results. Nevertheless, assessing the accuracy of our findings and the reproducibility of extracted features in other centers and device models and settings is necessary. One of the limitations of the current study is the examination of PET/CT images in a single center obtained from a single device model. Furthermore, assessing the dependability of the described highly consistent characteristics in differentiating between healthy/benign tissues and malignant/metastatic lesions is crucial in determining which characteristics are suitable for machine learning models based on PSMA-PET/CT.

Besides, it cannot be confidently stated that the current results would yield similar results on other real-life datasets of metastatic PCa, as radiomics features are generally influenced by various clinical and imaging-related factors. Therefore, we recommend using features from our analysis in future studies. Furthermore, the agreement rate between the said features and biopsy results must be determined in future studies. Ultimately, we conclude that three features, low gray-level emphasis, low gray-level run emphasis, and long-run low gray-level emphasis, have the highest reproducibility and potential for detecting metastatic PCa.

## REFERENCES

1. Spohn SK, Bettermann AS, Bamberg F, Benndorf M, Mix M, Nicolay NH, et al. Radiomics in prostate cancer imaging for a personalized treatment approach-current aspects of methodology and a systematic review on validated studies. Theranostics. 2021;11(16):8027.
2. Alongi P, Stefano A, Comelli A, Laudicella R, Scalisi S, Arnone G, et al. Radiomics analysis of 18F-Choline PET/CT in the prediction of disease outcome in high-risk prostate cancer: An explorative study on machine learning feature classification in 94 patients. European Radiology. 2021;31:4595-605.
3. Fuchsjäger M, Shukla-Dave A, Akin O, Barentsz J, Hricak H. Prostate cancer imaging. Acta radiologica. 2008;49(1):107-20.


**DOI:** 10.46121/pspc.52.4.6

4. Pasini G, Russo G, Mantarro C, Bini F, Richiusa S, Morgante L, et al. A Critical Analysis of the Robustness of Radiomics to Variations in Segmentation Methods in 18F-PSMA-1007 PET Images of Patients Affected by Prostate Cancer. Diagnostics. 2023;13(24):3640.
5. Hinzpeter R, Baumann L, Guggenberger R, Huellner M, Alkadhi H, Baessler B. Radiomics for detecting prostate cancer bone metastases invisible in CT: a proof-of-concept study. European radiology. 2022:1-10.
6. Zamboglou C, Bettermann AS, Gratzke C, Mix M, Ruf J, Kiefer S, et al. Uncovering the invisible—prevalence, characteristics, and radiomics feature–based detection of visually undetectable intraprostatic tumor lesions in 68 GaPSMA-11 PET images of patients with primary prostate cancer. European Journal of Nuclear Medicine and Molecular Imaging. 2021;48:1987-97.
7. Zang S, Ai S, Yang R, Zhang P, Wu W, Zhao Z, et al. Development and validation of 68Ga-PSMA-11 PET/CT-based radiomics model to detect primary prostate cancer. EJNMMI research. 2022;12(1):1-8.
8. Meng Y, Sun J, Qu N, Zhang G, Yu T, Piao H. Application of radiomics for personalized treatment of cancer patients. Cancer management and research. 2019;11:10851.
9. Bonett DG. Sample size requirements for estimating intraclass correlations with desired precision. Statistics in medicine. 2002;21(9):1331-5.
10. 10.Dutta A, Chan J, Haworth A, Dubowitz DJ, Kneebone A, Reynolds HM. Robustness of magnetic resonance imaging and positron emission tomography radiomic features in prostate cancer: Impact on recurrence prediction after radiation therapy. Phys Imaging Radiat Oncol. 2024;29:100530.
11. Kendrick J, Francis RJ, Hassan GM, Rowshanfarzad P, Ong JSL, Jeraj R, et al. Prospective inter- and intra-tracer repeatability analysis of radiomics features in [(68)Ga]Ga-PSMA-11 and [(18)F]F-PSMA-1007 PET scans in metastatic prostate cancer. Br J Radiol. 2023;96(1152):20221178.
12. Fedorov A, Beichel R, Kalpathy-Cramer J, Finet J, Fillion-Robin J-C, Pujol S, et al. 3D Slicer as an image computing platform for the Quantitative Imaging Network. Magnetic resonance imaging. 2012;30(9):1323-41.
13. Van Griethuysen JJ, Fedorov A, Parmar C, Hosny A, Aucoin N, Narayan V, et al. Computational radiomics system to decode the radiographic phenotype. Cancer research. 2017;77(21):e104-e7.
14. McGraw KO, Wong SP. Forming inferences about some intraclass correlation coefficients. Psychological methods. 1996;1(1):30.
15. Koo TK, Li MY. A guideline of selecting and reporting intraclass correlation coefficients for reliability research. Journal of chiropractic medicine. 2016;15(2):155-63.
16. Stefano A, Leal A, Richiusa S, Trang P, Comelli A, Benfante V, et al. Robustness of pet radiomics features: Impact of co-registration with mri. Applied Sciences. 2021;11(21):10170.
17. Cairone L, Benfante V, Bignardi S, Marinozzi F, Yezzi A, Tuttolomondo A, et al., editors. Robustness of radiomics features to varying segmentation algorithms in magnetic resonance images. International Conference on Image Analysis and Processing; 2022: Springer.


**DOI:** 10.46121/pspc.52.4.6

18. Traverso A, Wee L, Dekker A, Gillies R. Repeatability and reproducibility of radiomic features: a systematic review. International Journal of Radiation Oncology* Biology* Physics. 2018;102(4):1143-58.
19. Moazemi S, Erle A, Lütje S, Gaertner FC, Essler M, Bundschuh RA. Estimating the potential of radiomics features and radiomics signature from pretherapeutic PSMA-PET-CT scans and clinical data for prediction of overall survival when treated with 177Lu-PSMA. Diagnostics. 2021;11(2):186.
20. Zamboglou C, Carles M, Fechter T, Kiefer S, Reichel K, Fassbender TF, et al. Radiomic features from PSMA PET for non-invasive intraprostatic tumor discrimination and characterization in patients with intermediate- and high-risk prostate cancer - a comparison study with histology reference. Theranostics. 2019;9(9):2595-605.
21. Khurshid Z, Ahmadzadehfar H, Gaertner FC, Papp L, Zsóter N, Essler M, Bundschuh RA. Role of textural heterogeneity parameters in patient selection for 177Lu-PSMA therapy via response prediction. Oncotarget. 2018;9(70):33312.
22. Alongi P, Stefano A, Comelli A, Laudicella R, Scalisi S, Arnone G, et al. Radiomics analysis of 18F-Choline PET/CT in the prediction of disease outcome in high-risk prostate cancer: an explorative study on machine learning feature classification in 94 patients. Eur Radiol. 2021;31(7):4595-605.
23. Leijenaar RT, Nalbantov G, Carvalho S, Van Elmpt WJ, Troost EG, Boellaard R, et al. The effect of SUV discretization in quantitative FDG-PET Radiomics: the need for standardized methodology in tumor texture analysis. Scientific reports. 2015;5(1):11075.
24. Hatt M, Majdoub M, Vallières M, Tixier F, Le Rest CC, Groheux D, et al. FDG PET uptake characterization through texture analysis: investigating the complementary nature of heterogeneity and functional tumor volume in a multi-cancer site patient cohort.
25. Orlhac F, Soussan M, Maisonobe J-A, Garcia CA, Vanderlinden B, Buvat I. Tumor texture analysis in 18F-FDG PET: relationships between texture parameters, histogram indices, standardized uptake values, metabolic volumes, and total lesion glycolysis. Journal of Nuclear Medicine. 2014;55(3):414-22.


**DOI:** 10.46121/pspc.52.4.6

Power System Protection and Control
ISSN:1674-3415

**Tables**

**Table 1. Features extracted from PET-CT images based on their categories**

| Extracted features | | | | | | |
|---|---|---|---|---|---|---|
| First-order statistics (FOS) | **Gray-level co-occurrence matrix (GLCM)** | **Gray-level run length matrix (GLRLM)** | **Shape and morphological features** | **Gray-Level Size Zone Matrix (GLSZM)** | **Gray-level dependence matrix (GLDM)** | **Neighboring gray-tone difference matrix (NGTDM)** |
| **Energy** | Autocorrelation | Short-run emphasis (SRE) | VoxelVolume | Small Area Emphasis (SAE) | Small Dependence Emphasis (SDE) | Coarseness |
| **Total Energy** | Joint average | Long-run emphasis (LRE) | MeshVolume | Large Area Emphasis (LAE) | Large Dependence Emphasis (LDE) | Contrast |
| **Entropy** | Cluster prominence | Gray-Level Non-Uniformity (GLN) | Surface area | Gray-Level Non-Uniformity (GLN) | Dependence Non-Uniformity (DN) | Busyness |
| **Minimum** | Cluster shade | Gray-Level Non-Uniformity Normalized (GLNN) | Surface area to volume ratio | Size-Zone Non-Uniformity (SZN) | Dependence Non-Uniformity Normalized (DNN) | Complexity |
| **10th percentile** | Cluster tendency | Run Length Non-Uniformity (RLN) | Sphericity | Size-Zone Non-Uniformity Normalized (SZNN) | Gray-level variance (GLV) | Strength |
| **90th percentile** | Contrast | Run Length Non-Uniformity Normalized (RLNN) | Spherical disproportion | Zone Percentage (ZP) | Dependence variance (DV) | |
| **Maximum** | Correlation | Run percentage (RP) | Maximum 3D diameter | Gray-level variance (GLV) | Dependence entropy (DE) | |
| **Mean** | Difference average | Gray-level variance (GLV) | Maximum 2D diameter (slice) | Zone variance (ZV) | Low Gray-Level Emphasis (LGLE) | |
| **Median** | Difference entropy | Run variance (RV) | Maximum 2D diameter (column) | Zone entropy (ZE) | High Gray-Level Emphasis (HGLE) | |
| **Interquartile range** | Difference variance | Run entropy (RE) | Maximum 2D diameter (row) | Low Gray-Level Zone Emphasis (LGLZE) | Small Dependence Low Gray-Level Emphasis (SDLGLE) | |


**DOI:** 10.46121/pspc.52.4.6

| | | | | | |
|---|---|---|---|---|---|
| **Range** | Joint energy | Low Gray-Level Run Emphasis (LGLRE) | Major axis | High Gray-Level Zone Emphasis (HGLZE) | Small Dependence High Gray-Level Emphasis (SDHGLE) |
| **Mean absolute deviation (MAD)** | Joint entropy | High Gray-Level Run Emphasis (HGLRE) | Minor axis | Small Area Low Gray-Level Emphasis (SALGLE) | Large Dependence Low Gray-Level Emphasis (LDLGLE) |
| **Robust mean absolute deviation (rMAD)** | Informal measure of correlation (IMC) 1 | Short-Run Low Gray-Level Emphasis (SRLGLE) | Least axis | Small Area High Gray-Level Emphasis (SAHGLE) | Large Dependence High Gray-Level Emphasis (LDHGLE) |
| **Root mean squared (RMS)** | Informal measure of correlation (IMC) 2 | Short-Run High Gray-Level Emphasis (SRHGLE) | Elongation | Large Area Low Gray-Level Emphasis (LALGLE) | |
| **Standard deviation** | Inverse difference moment (IDM) | Long-Run Low Gray-Level Emphasis (LRLGLE) | Flatness | Large Area High Gray-Level Emphasis (LAHGLE) | |
| **Skewness** | Inverse Difference Moment Normalized (IDMN) | Long-Run High Gray-Level Emphasis (LRHGLE) | | | |
| **Kurtosis** | Inverse difference (ID) | | | | |
| **Variance** | Inverse Difference Normalized (IDN) | | | | |
| **Uniformity** | Inverse variance | | | | |
| | Maximum probability | | | | |
| | Sum average | | | | |
| | Sum entropy | | | | |
| | Sum of squares | | | | |


**DOI:** 10.46121/pspc.52.4.6

Power System Protection and Control
ISSN:1674-3415

**Table 2. Demographic and clinical characteristics of participants**

| Characteristic | Participants No. = 150 |
|---|---|
| Age (years)**, mean ± SD** | 68.6 ± 7.08 |
| Weight (Kilograms)**, mean ± SD** | 73.19 ± 10.46 |
| PSA level at diagnosis (ng/ml)**, mean ± SD** | 6.5 ± 12.2 |
| Mediastinal Blood Pool SUV**, mean ± SD** | 1.24 ± 0.27 |
| Current staging**, No. (%)** | |
| **Unknown** | 1 (0.7%) |
| **Initial staging** | 30 (20%) |
| **Restaging** | 119 (79.3%) |
| History of prostatectomy**, No. (%)** | |
| **Unspecified** | 4 (2.7% ) |
| **Negative** | 56 (37.3%) |
| **Positive** | 90 (60%) |
| Latest PSA level**, No. (%)** | |
| **Below 20 ng/ml** | 132 (93%) |
| **Above 20 ng/ml** | 10 (7%) |

Abbreviations: SUV, Standardized Uptake Value; PSA, Prostate Specific Antigen

**Table 3. Intraclass correlation coefficient of the extracted features**

| Feature | ICC | 95% CI of ICC | | P-value |
|---|---|---|---|---|
| | | lower limit | upper limit | |
| **First-order statistics (FOS)** | | | | |
| Energy | 0.241 | -3.972 | 0.999 | 0.273 |
| Total Energy | 0.241 | -3.972 | 0.999 | 0.273 |
| Entropy | 0.197 | -4.261 | 0.999 | 0.286 |
| Minimum | 0.552 | -1.937 | 1 | 0.161 |
| $10^{th}$ percentile | 0.366 | -3.156 | 0.999 | 0.233 |
| $90^{th}$ percentile | -0.487 | -8.744 | 0.998 | 0.428 |
| Maximum | -22.84 | -159.306 | 0.975 | 0.841 |
| Mean | -3.413 | -27.921 | 0.995 | 0.643 |
| Median | -7.071 | -51.895 | 0.992 | 0.731 |
| Interquartile range | 0.421 | -2.794 | 0.999 | 0.213 |
| Range | -9.062 | -64.942 | 0.99 | 0.758 |
| Mean absolute deviation (MAD) | 0.11 | -4.831 | 0.999 | 0.31 |
| Robust Mean absolute deviation (rMAD) | 0.373 | -3.106 | 0.999 | 0.23 |
| Root Mean squared (RMS) | -2.438 | -21.534 | 0.996 | 0.6 |
| Skewness | -3.437 | -28.079 | 0.995 | 0.643 |
| Kurtosis | 0.165 | -4.474 | 0.999 | 0.295 |
| Variance | 0.21 | -4.18 | 0.999 | 0.283 |
| Uniformity | 0.682 | -1.081 | 1 | 0.101 |
| **Gray-level co-occurrence matrix (GLCM)** | | | | |
| Autocorrelation | 0.254 | -3.886 | 0.999 | 0.269 |
| Joint average | -0.285 | -7.424 | 0.999 | 0.395 |
| Cluster prominence | 0.278 | -3.734 | 0.999 | 0.262 |
| Cluster shade | -1.727 | -16.871 | 0.997 | 0.556 |
| Cluster tendency | 0.185 | -4.343 | 0.999 | 0.29 |
| Contrast | -4.138 | -32.675 | 0.995 | 0.667 |
| Correlation | -10.352 | -73.401 | 0.988 | 0.772 |
| Difference average | -2.797 | -23.884 | 0.996 | 0.617 |
| Difference entropy | -2.074 | -19.145 | 0.997 | 0.579 |
| Difference variance | -270.435 | -1777.92 | 0.722 | 0.953 |
| Joint energy | 0.478 | -2.42 | 0.999 | 0.191 |


**DOI:** 10.46121/pspc.52.4.6

| | | | | |
|---|---|---|---|---|
| Joint entropy | 0.303 | -3.567 | 0.999 | 0.254 |
| Informal measure of correlation (IMC) 1 | -21.412 | -145.883 | 0.977 | 0.836 |
| Informal measure of correlation (IMC) 2 | -7.586 | -55.271 | 0.991 | 0.739 |
| Inverse difference moment (IDM) | -0.017 | -5.667 | 0.999 | 0.341 |
| Inverse Difference Moment Normalized (IDMN) | -793.773 | -5207.76 | 0.186 | 0.972 |
| Inverse difference (ID) | -0.307 | -7.567 | 0.999 | 0.399 |
| Inverse Difference Normalized (IDN) | -50.082 | -333.78 | 0.948 | 0.891 |
| Inverse variance | -4.581 | -35.578 | 0.994 | 0.68 |
| Maximum probability | 0.561 | -1.874 | 1 | 0.157 |
| Sum average | -0.285 | -7.424 | 0.999 | 0.395 |
| Sum entropy | 0.238 | -3.995 | 0.999 | 0.274 |
| Sum of squares | 0.175 | -4.404 | 0.999 | 0.292 |
| **Gray-level run length matrix (GLRLM)** | | | | |
| Short-run emphasis (SRE) | 0.478 | -2.419 | 0.999 | 0.191 |
| Long-run emphasis (LRE) | 0.347 | -3.28 | 0.999 | 0.24 |
| Gray-Level Non-Uniformity (GLN) | 0.408 | -0.802 | 0.929 | 0.167 |
| Gray-Level Non-Uniformity Normalized (GLNN) | -0.208 | -6.918 | 0.999 | 0.381 |
| Run Length Non-Uniformity (RLN) | 0.588 | -1.342 | 1 | 0.132 |
| Run Length Non-Uniformity Normalized (RLNN) | 0.327 | -3.413 | 0.999 | 0.246 |
| Run percentage (RP) | 0.521 | -2.14 | 1 | 0.174 |
| Run variance (RV) | 0.355 | -3.228 | 0.999 | 0.237 |
| Run entropy (RE) | -0.106 | -6.249 | 0.999 | 0.36 |
| Low Gray-Level Run Emphasis (LGLRE) | 0.799 | -0.349 | 1 | 0.047 |
| High Gray-Level Run Emphasis (HGLRE) | 0.26 | -3.848 | 0.999 | 0.268 |
| Short-Run Low Gray-Level Emphasis (SRLGLE) | 0.79 | -0.412 | 1 | 0.052 |
| Short-Run High Gray-Level Emphasis (SRHGLE) | 0.269 | -3.789 | 0.999 | 0.265 |
| Long-Run Low Gray-Level Emphasis (LRLGLE) | 0.801 | -0.307 | 1 | 0.045 |
| Long-Run High Gray-Level Emphasis (LRHGLE) | -0.116 | -6.313 | 0.999 | 0.362 |
| **Shape and morphological features** | | | | |
| Voxel Volume | 0.588 | -1.697 | 1 | 0.145 |
| Mesh Volume | 0.589 | -1.697 | 1 | 0.145 |
| Surface area | 0.533 | -2.06 | 1 | 0.169 |


**DOI:** 10.46121/pspc.52.4.6

| | | | | |
|---|---|---|---|---|
| Surface area to volume ratio | 0.143 | -4.616 | 0.999 | 0.301 |
| Sphericity | -26.783 | -181.083 | 0.972 | 0.853 |
| Maximum 3D diameter | -0.028 | -5.912 | 0.999 | 0.345 |
| Maximum 2D diameter (slice) | -0.14 | -6.472 | 0.999 | 0.367 |
| Maximum 2D diameter (column) | 0.401 | -3.025 | 0.999 | 0.223 |
| Maximum 2D diameter (row) | -3.589 | -29.855 | 0.995 | 0.65 |
| Major axis | -0.795 | -10.761 | 0.998 | 0.47 |
| Minor axis | 0.628 | -1.503 | 1 | 0.129 |
| Least axis | -0.536 | -9.332 | 0.998 | 0.437 |
| Elongation | .359c | -3.199 | 0.999 | 0.235 |
| Flatness | -0.083 | -6.096 | 0.999 | 0.356 |
| **Gray-Level Size Zone Matrix (GLSZM)** | | | | |
| Small Area Emphasis (SAE) | -2.716 | -23.351 | 0.996 | 0.613 |
| Large Area Emphasis (LAE) | 0.452 | -2.591 | 0.999 | 0.202 |
| Gray-Level Non-Uniformity (GLN) | 0.408 | -0.802 | 0.929 | 0.167 |
| Gray-Level Non-Uniformity Normalized (GLNN) | -0.208 | -6.918 | 0.999 | 0.381 |
| Size-Zone Non-Uniformity (SZN) | 0.23 | -4.049 | 0.999 | 0.277 |
| Size-Zone Non-Uniformity Normalized (SZNN) | -1.505 | -15.415 | 0.997 | 0.539 |
| Zone Percentage (ZP) | -0.941 | -11.721 | 0.998 | 0.487 |
| Zone variance (ZV) | 0.452 | -2.593 | 0.999 | 0.202 |
| Zone entropy (ZE) | -5.042 | -38.595 | 0.994 | 0.691 |
| Low Gray-Level Zone Emphasis (LGLZE) | 0.084 | -5.001 | 0.999 | 0.317 |
| High Gray-Level Zone Emphasis (HGLZE) | 0.261 | -3.843 | 0.999 | 0.267 |
| Small Area Low Gray-Level Emphasis (SALGLE) | -0.495 | -8.797 | 0.998 | 0.429 |
| Small Area High Gray-Level Emphasis (SAHGLE) | 0.276 | -3.748 | 0.999 | 0.263 |
| Large Area Low Gray-Level Emphasis (LALGLE) | -0.495 | -8.797 | 0.998 | 0.429 |
| Large Area High Gray-Level Emphasis (LAHGLE) | 0.276 | -3.748 | 0.999 | 0.263 |
| **Gray-level dependence matrix (GLDM)** | | | | |
| Small Dependence Emphasis (SDE) | -0.856 | -11.167 | 0.998 | 0.477 |
| Large Dependence Emphasis (LDE) | 0.486 | -2.368 | 0.999 | 0.188 |
| Dependence Non-Uniformity (DN) | 0.452 | -2.118 | 0.999 | 0.189 |


**DOI:** 10.46121/pspc.52.4.6

| | | | | |
|---|---|---|---|---|
| Dependence Non-Uniformity Normalized (DNN) | -2.002 | -18.675 | 0.997 | 0.575 |
| Dependence variance (DV) | 0.47 | -2.475 | 0.999 | 0.195 |
| Dependence entropy (DE) | 0.212 | -4.166 | 0.999 | 0.282 |
| Low Gray-Level Emphasis (LGLE) | 0.906 | 0.462 | 1 | 0.003 |
| High Gray-Level Emphasis (HGLE) | 0.26 | -3.849 | 0.999 | 0.268 |
| Small Dependence Low Gray-Level Emphasis (SDLGLE) | -203.302 | -1337.951 | 0.791 | 0.945 |
| Small Dependence High Gray-Level Emphasis (SDHGLE) | 0.292 | -3.641 | 0.999 | 0.258 |
| Large Dependence Low Gray-Level Emphasis (LDLGLE) | 0.747 | -0.66 | 1 | 0.07 |
| **Neighboring gray-tone difference matrix (NGTDM)** | | | | |
| Coarseness | -7.119 | -55.317 | 0.992 | 0.733 |
| Contrast | -4.138 | -32.675 | 0.995 | 0.667 |
| Busyness | 0.522 | -2.132 | 1 | 0.174 |
| Complexity | -0.109 | -6.27 | 0.999 | 0.361 |
| Strength | -6.866 | -50.555 | 0.992 | 0.728 |

Abbreviations: ICC, Intraclass correlation coefficient; CI, Confidence interval.


**DOI:** 10.46121/pspc.52.4.6

Power System Protection and Control
ISSN:1674-3415

**Figures**

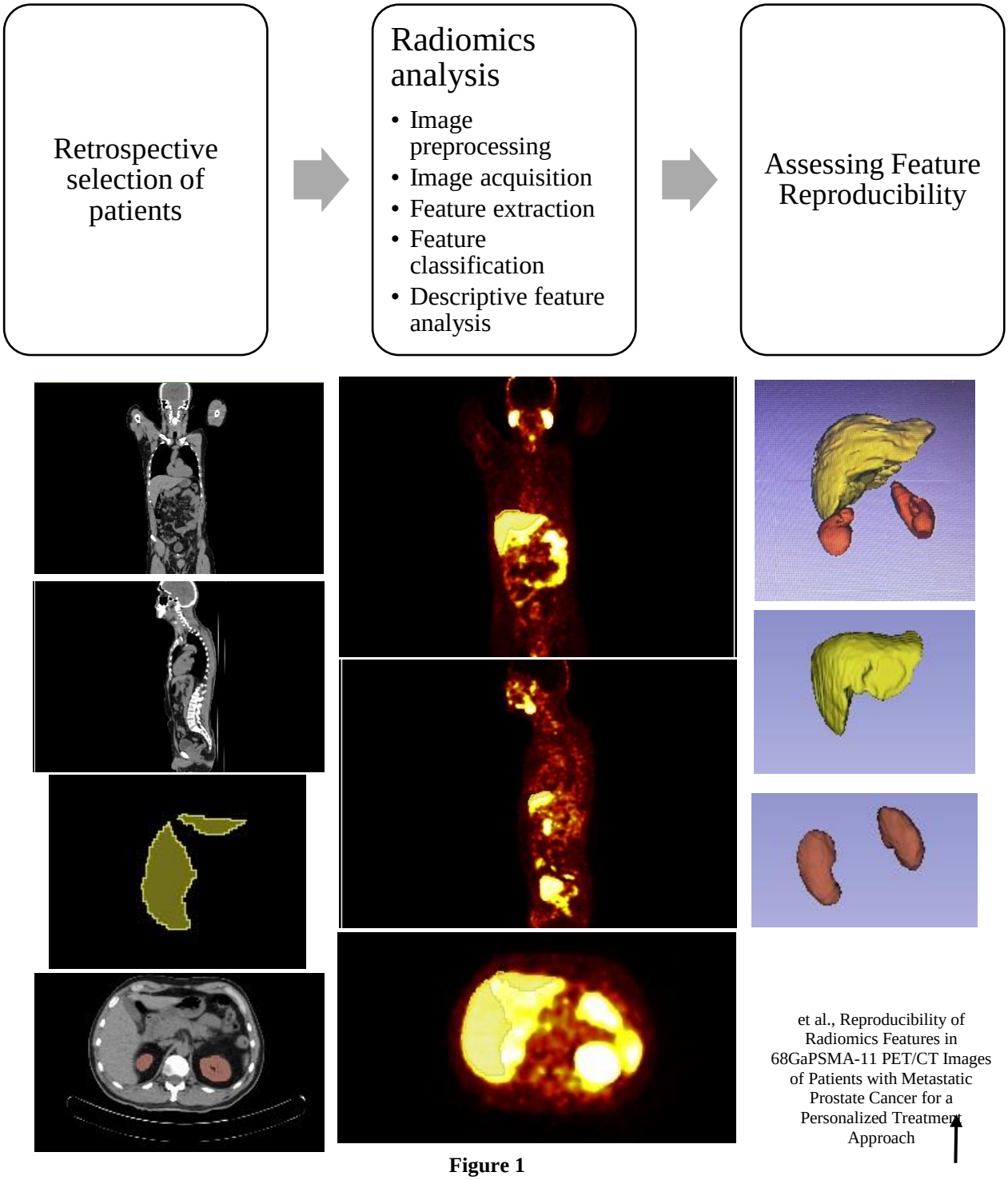


**Figure 1**



**DOI:** 10.46121/pspc.52.4.6

Power System Protection and Control
ISSN:1674-3415

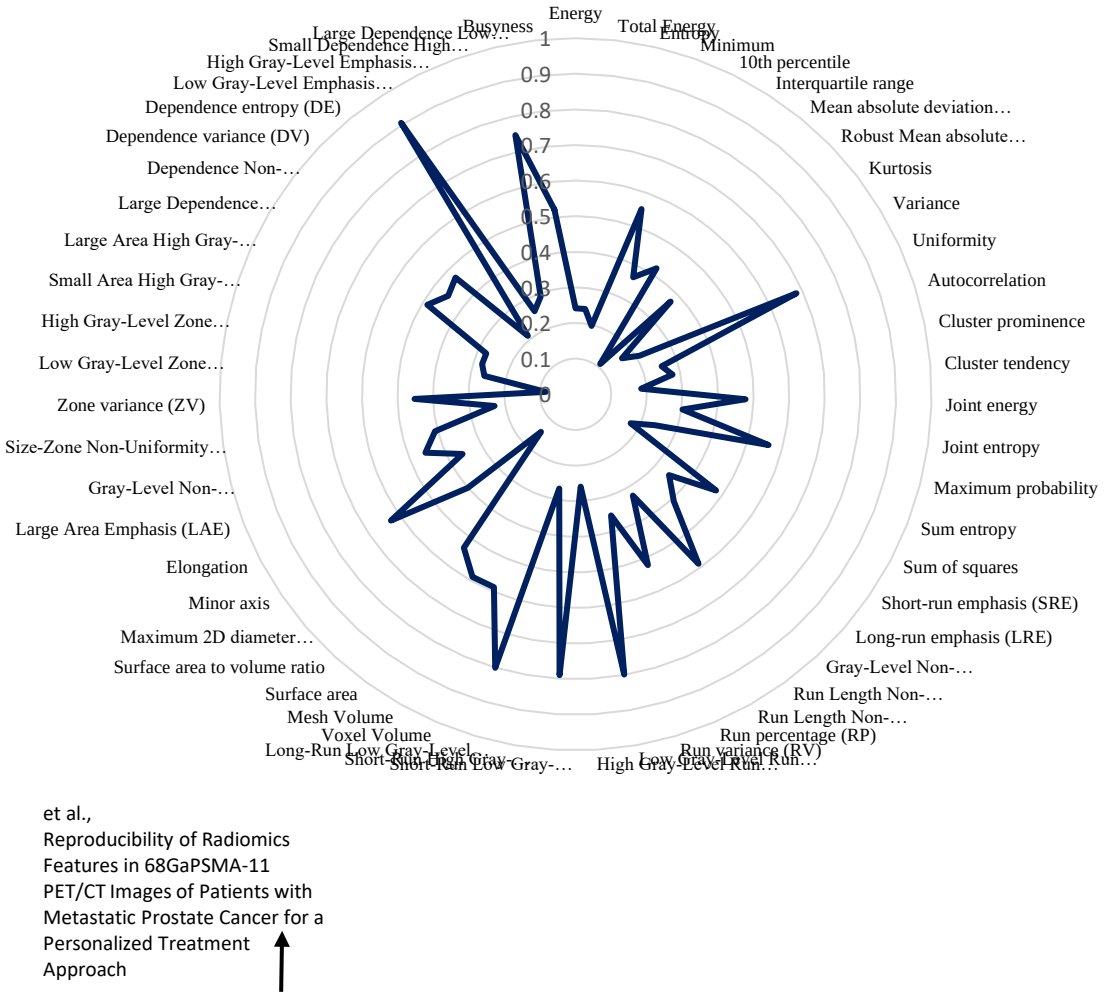


et al.,
Reproducibility of Radiomics Features in 68GaPSMA-11 PET/CT Images of Patients with Metastatic Prostate Cancer for a Personalized Treatment Approach

**Figure 2**


**DOI:** 10.46121/pspc.52.4.6

Power System Protection and Control
ISSN:1674-3415

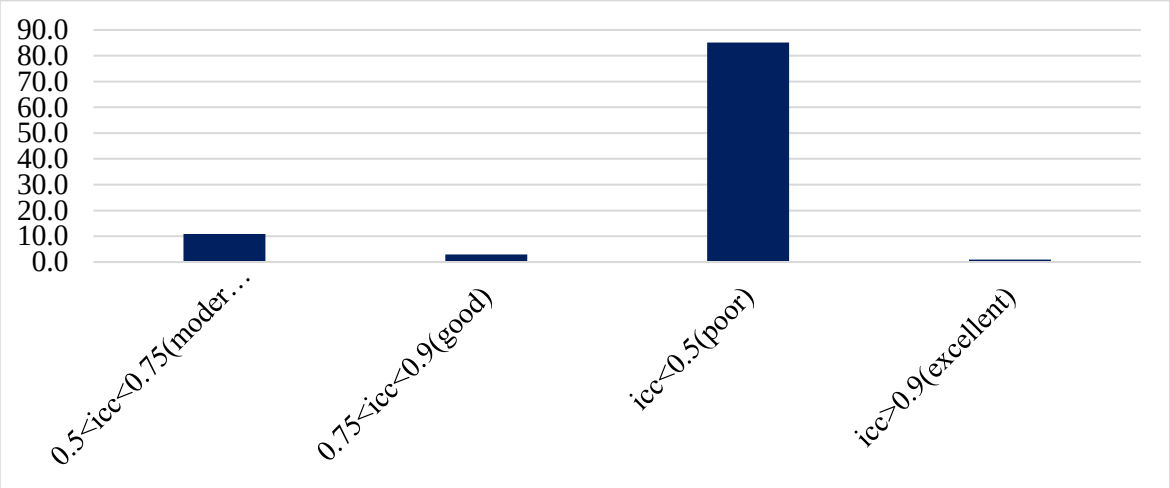


**Figure 3**

**Figure legends**
**Figure 1.** Study's phases and steps, along with PET/CT images used for segmentation
**Figure 2.** Intraclass correlation coefficient (ICC) of the most repeatable extracted radiomics features
**Figure 3.** Number of features with excellent, good, moderate, and poor reproducibility

https://actu.epfl.ch/news/tracking-facial-features-to-make-driving-safer-and/}.


**DOI:** 10.46121/pspc.52.4.6